Split Ring FSS Reflectarray with Spiral Phase Distribution

Zelenchuk, D., Fusco, V., & Malyuskin, O. (2013). Split Ring FSS Reflectarray with Spiral Phase Distribution. In 2013 7th European Conference on Antennas and Propagation (EuCAP),. (pp. 2709 - 2713). Institute of Electrical and Electronics Engineers (IEEE).

Published in:
2013 7th European Conference on Antennas and Propagation (EuCAP),

Document Version:
Early version, also known as pre-print

Queen's University Belfast - Research Portal:
Link to publication record in Queen's University Belfast Research Portal

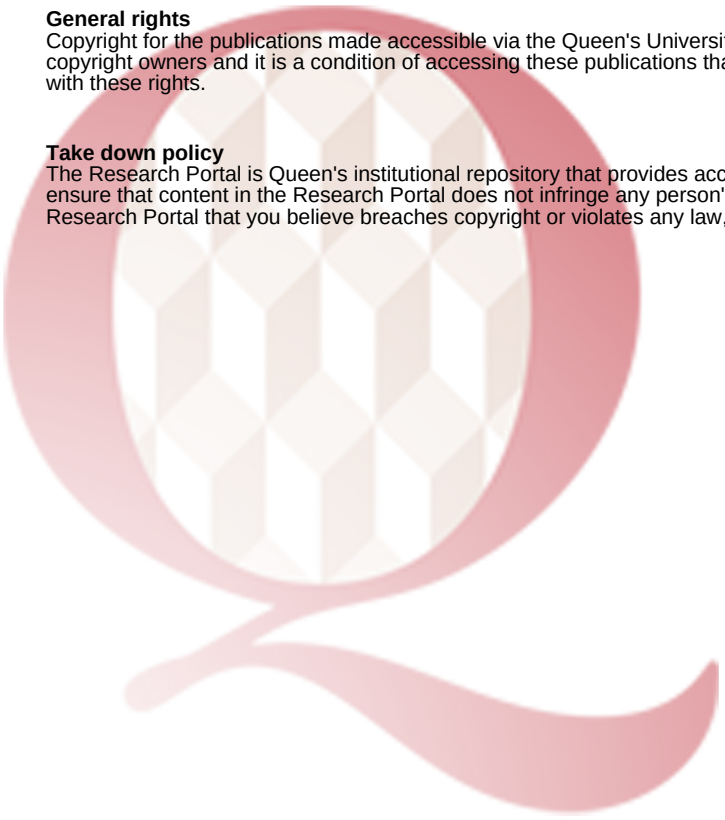

Split Ring FSS Reflectarray with Spiral Phase Distribution

Split Ring Reflectarray FSS with Spiral Phase Distribution

Dmitry Zelenchuk, Vincent Fusco and Oleksandr Malyuskin
The Institute of Electronics, Communications and Information Technology,
Queen's University of Belfast
Belfast, United Kingdom
d.zelenchuk@qub.ac.uk, v.fusco@qub.ac.uk, o.malyuskin@qub.ac.uk

***Abstract*—The paper reports of a flat spiral phase plate structure based on reflectarray frequency selective surface, FSS, technology for the generation of helical far-field radiation patterns with circular polarization (CP) properties. Double split ring slot FSS is used as a means for adjusting the phase across the reflectarray. Simulations presented demonstrate generation of reflected helical beams at 10 GHz for CP wave incident on the structure. The far-field measurements are in a good agreement with the simulations and demonstrate a null of -11dB in the centre of the radiation pattern attributed to the helical wavefront.**

***Index Terms*—spiral phase plate; frequency selective surface; reflectarray**

I. INTRODUCTION

There is a significant interest in generation of helical beams with non-zero orbital angular momentum [1]. They find application in advanced optics for imaging, [2] , and may have significant future potential for enhanced spectrally efficient radio communications, [3]. Such helical beams can be generated with non-planar structures such as the machined spiral dielectric cylinder [4], spiral phase reflector with discrete step [3] or helicoidal parabolic antenna [5]. It was suggested in [6] that a planar spiral phase plate can be used for the transformation of a Gaussian beam into a helical beam, however the proposed approach involved variation in both permittivity and permeability throughout the plate and the approach does not constitute a reduction in manufacturing complexity compared with the structure in Figure 1.

In this paper we report a planar spiral phase plate which uses a quasi periodic reflectarray FSS whose unit cell elements are orientated to produce the same wave front transformation as is made by the 3D spiral phase plate in [4].

The paper is organized as follows: first the principle of operation of a 3D dielectric spiral phase plate is explained, and then the theory behind the proposed periodic reflecting FSS phase shifter is given. Based on that theory a design procedure for finite structure is explained and its characteristics are discussed. Next section describes the measurement setup, and compares the obtained radiation pattern with the one predicted with the full-wave simulations. Main aspects of the paper are summarized in Conclusions.

This work was conducted under the UK Engineering and Physical Science Research council grant EP/H049606/1 and the Leverhulme Trust Research Project Grant F/00 203/U-Phase Conjugate Wireless Communication.

II. THEORY

A. Spiral Phase Plate

A spiral phase plate can be milled from a solid cylindrical dielectric block of fixed dielectric constant ε by forming a helix with a step discontinuity, see Figure 1.

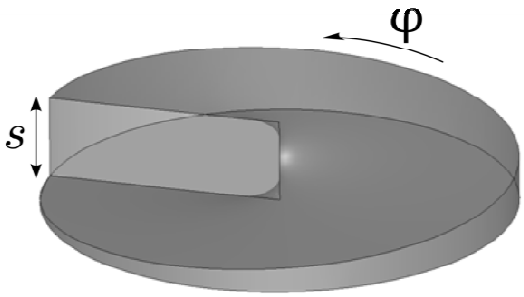

Figure 1. Dielectric cylinder spiral phase plate.

A plane wavefront of wavelength λ passing through the structure is subject to a phase delay, ψ, which depends on azimuthal angle, φ, [4],

$$\psi = \frac{\left(\sqrt{\varepsilon} - 1\right)s}{\lambda}\varphi \tag{1}$$

In order to produce a helical exit beam the total phase delay around the phase plate should be $2\,\pi l, l \in \mathbb{N}$. Thus to produce a the helical exit beam the physical height of the step should be

$$s = \frac{l\,\lambda}{\sqrt{\varepsilon} - 1} \tag{2}$$

The effect that such a structure has on an incident Gaussian beam is illustrated in Figure 2. Once the beam passes the spiral phase plate it transforms into a Laguerre-Gaussian beam with a null in the centre and helical exit wavefront [1].

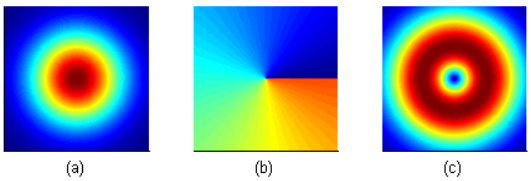

Figure 2. Generation of helical beam: (a) amplitude of incident Gaussian beam, (b) spiral phase plate phase distribution, (c) amplitude of resultant Laguerre-Gaussian beam.

B. Reflecting FSS phase shifter

In order to implement the planar structure with the properties equivalent to the spiral phase plate we propose a reflecting FSS with rotational phase shift. The fundamental paradigm of the rotational phase shift dates back to optical wave plates [7] and waveguide phase shifters [8] and has since been developed for quasi periodic lenses [9] and reflectarrays [10], [11]. Below we discuss the basic principle of operation of the phase shifter.

Let us assume that a plane wave is normally incident onto the double slot periodic structure with unit cell given in Figure 3 and that the unit cell can rotate about its origin by angle θ_r . On applying the Jones calculus [7] one can derive the reflected field from the FSS as

$$\boldsymbol{E}_R = \begin{pmatrix} \cos\theta_r & -\sin\theta_r \\ \sin\theta_r & \cos\theta_r \end{pmatrix} \begin{pmatrix} \Gamma_{x'} & 0 \\ 0 & \Gamma_{y'} \end{pmatrix} \begin{pmatrix} \cos\theta_r & \sin\theta_r \\ -\sin\theta_r & \cos\theta_r \end{pmatrix} \boldsymbol{E}_i$$

where $\boldsymbol{E}_i$ is the incident field vector with x and y components, $\Gamma_{x'}$ and $\Gamma_{y'}$ are the reflection coefficients along the primed coordinates, shown in Figure 3.

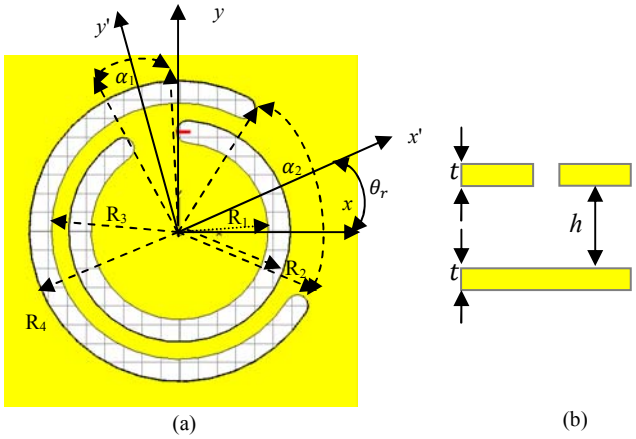

Figure 3. Double layer structure under test: (a) top view, (b) side view.

If the FSS is designed to yield $\Gamma_{x'} = -\Gamma_{y'}$ the reflected field can be expressed as

$$\boldsymbol{E}_R = \Gamma_{x'} \begin{pmatrix} \cos 2\theta_r & \sin 2\theta_r \\ \sin 2\theta_r & -\cos 2\theta_r \end{pmatrix} \boldsymbol{E}_i \qquad (3)$$

For a CP incident wave $\boldsymbol{E}_i = {}^1\!/_2 \begin{pmatrix} 1 \\ \pm j \end{pmatrix} e^{-jkz}$ it follows from (5) that the reflected wave should be

$$\boldsymbol{E}_R = \Gamma_{x'} e^{\pm j2\theta_r} \frac{1}{2} \begin{pmatrix} 1 \\ \mp j \end{pmatrix} e^{jkz} \qquad (4)$$

It follows from (4) that upon reflecting from the FSS an incident CP wave gains a phase shift of $2\theta_r$, and experience reflection loss defined by $\Gamma_{x'}$.

Notably, the sign of imaginary unit in (4) has changed in comparison to the incident field. However, the hand of polarisation remains the same as the direction of propagation changes to the opposite upon reflection. This is contrary to the conventional perfect conductor reflector for which the polarisation changes [12].

III. DESIGN

A. Unit cell design

The unit cell of the proposed structure is shown in Figure 3. The dimensions of the structure are optimized to fulfil the conditions derived above at the specified operating frequency of 10 GHz. The optimal dimensions of the unit cell are given in the Table I. The unit cell is square with a period of 19 mm.

The structure was simulated with CST Microwave Studio and the reflection coefficients for normally incident plane waves linearly polarised along x and y axes were obtained. It follows from the simulations that there is almost no energy converted into the opposite polarisation upon reflection as the amplitude of the corresponding reflection coefficients is below -25 dB, see Figure 4. Another important result is that the phase difference between the reflection coefficients is close to 180° in the 8% band with centre at 10 GHz, see Figure 5. The phase deviation within the band is 20°.

The results were combined to obtain the reflection coefficient for normally incident left hand circularly polarised wave [9], see Figure 6. One can observe that in the vicinity of 10 GHz the almost all the energy reflected into the wave with the same hand of polarisation. Most importantly the circularly polarized response has distinct frequency selective nature with the operational bandwidth determined by the phase response of the linearly polarised waves.

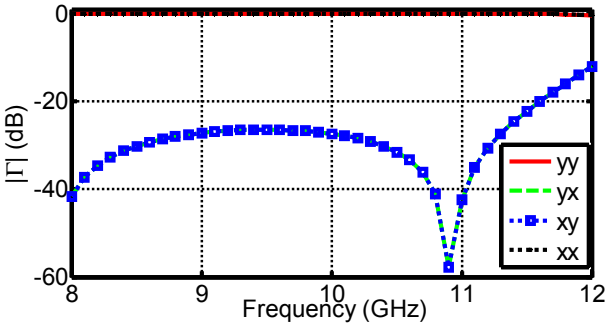

Figure 4. Simulated reflection amplitude for normally incident waves linearly polarised along x and y axes .

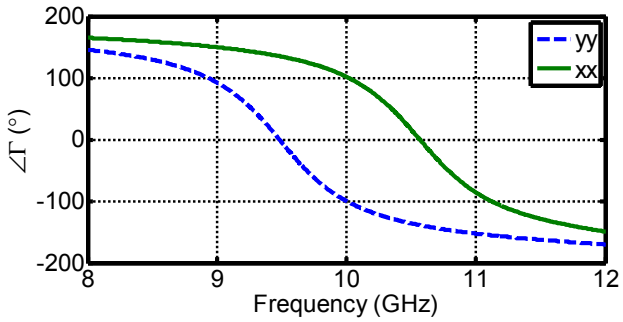

Figure 5. Simulated reflection phase for normally incident waves linearly polarised along *x* and *y* axes .

TABLE I. PARAMETERS OF THE UNIT CELL

R_1 , mm	R_2, mm	R_3, mm	R_4, mm	α_1,°	α_2,°	h, mm	t, mm
4.7	5.9	6.8	8	21	95	7.5	1

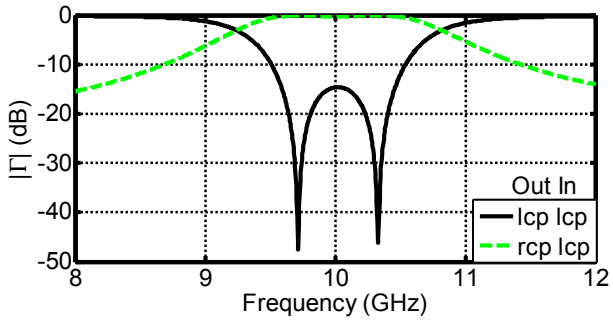

Figure 6. Simulated reflection amplitude for normal incidence of left hand circularly polarized wave (no rotation applied) .

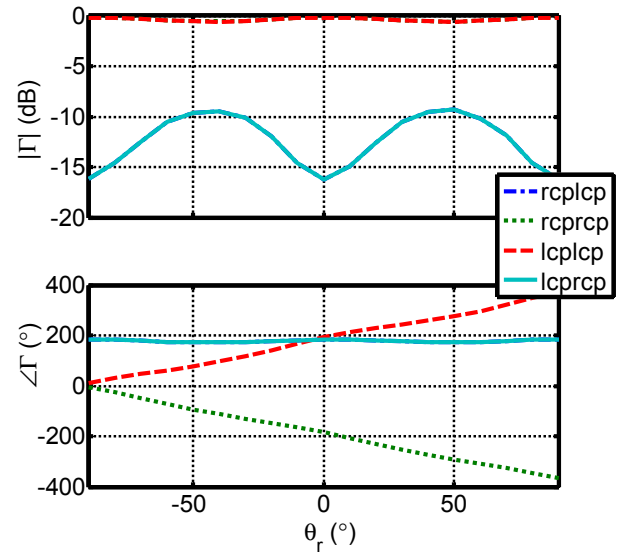

Figure 7. Simulated reflection amplitude and phase variation with rotation angle for normal incidence of circularly polarized waves at 10GHz.

As predicted in the precious section, the structure with such properties should produce a phase shift upon rotation of the element within the unit cell. The simulated amplitude and phase responses of the periodic structure when illuminated at normal incidence with a CP wave are shown in Figure 7, respectively, as the unit cell is rotated. From the simulated results one can conclude that the reflected wave preserves its hand opposite to the case of perfectly conducting mirror. The study also shows that the CP wave upon reflection from the structure gains a phase shift twice that of the rotation angle. The cross-polarization conversion level is better than 10 dB.

B. Finite 10x10 reflectarray

Based on the periodic FSS discussed above a 10x10 quasi-periodic reflectarray structure with spiral phase distribution and the dimensions given in Table I is proposed.

Analytically the spiral phase distribution can be written as follows

$$\psi(x,y)=\begin{cases}\tan^{-1}\frac{y}{x}, x>0, y>0\\ \tan^{-1}\frac{y}{x}+\pi, x<0\\ \tan^{-1}\frac{y}{x}+2\pi, x>0, y\le 0\end{cases} \quad (5)$$

Employing (5) at the centres of each unit cell element we present the required resulting phase rotation distribution in Table II. Each element of the array is then rotated in order to produce the necessary phase shift. The centre of the array is at (*x*=0 mm, *y*=0 mm).

TABLE II. SPIRAL PHASE SHIFT DISTRIBUTION IN DEGREES ACROSS THE SURFACE

x, mm / y, mm	-85.5	-66.5	-47.5	-28.5	-9.5	9.5	28.5	47.5	66.5	85.5
85.5	135	127.9	119.1	108.4	96.3	83.7	71.6	60.9	52.1	45
66.5	142	135	126	113	98	82	67	55	45	38
47.5	151	145	135	121	101	79	59	45	36	29
28.5	162	157	149	135	108	72	45	31	23	18
9.5	174	172	169	162	135	45	18	11	8	6
-9.5	186	188	191	198	225	315	342	349	352	354
-28.5	198	203	211	225	252	288	315	329	337	342
-47.5	209	216	225	239	259	281	301	315	325	331
-66.5	218	225	235	247	262	278	293	306	315	322
-85.5	225	232	241	252	264	276	288	299	308	315

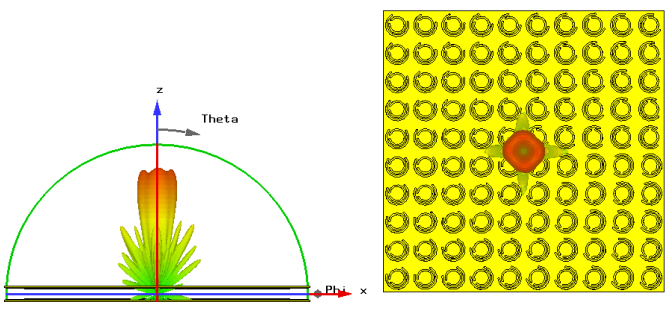

Figure 8. Simulated scattered LHCP field from the structure excited by LHCP plane wave at 10GHz.

The finite structure with the phase shifts induced in accordance with Table II was simulated in CST Microwave Studio. The simulated scattered LHCP field upon excitation with normally incident LHCP plane wave at 10 GHz is shown in Figure 8. As one can observe the main beam of reflected field contains null in the centre, which is the result of the spiral phase delay introduced by the screen.

IV. MEASUREMENTS

The reflectarray was manufactured from 1 mm thick aluminium. The slots were drilled on the top metal sheet and the bottom sheet remained intact. Both plates were secured with plastic screws and gaskets to maintain the required separation between the plates.

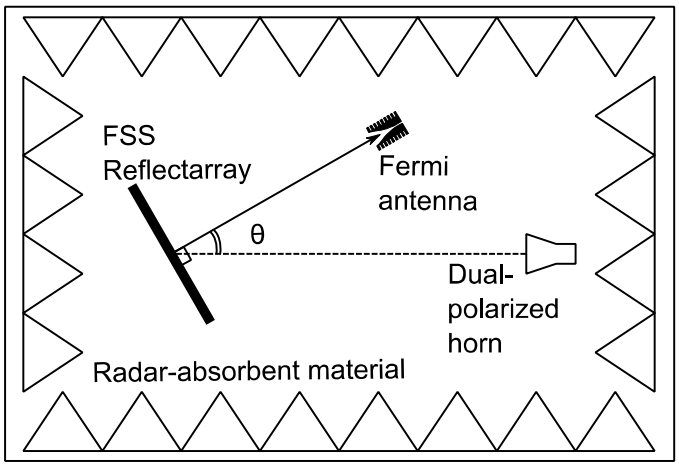

Figure 9. Bi-static measurement setup.

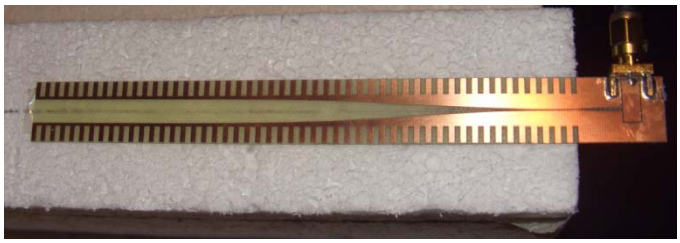

(a)

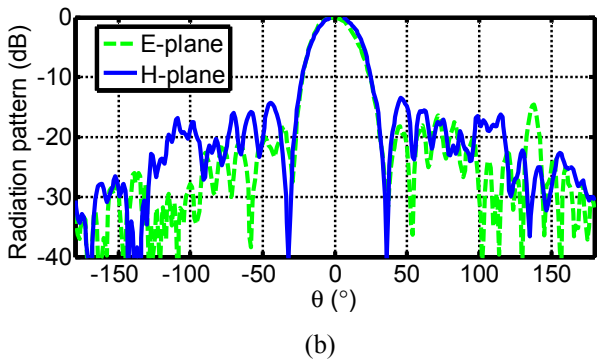

(b)

Figure 10. Fermi antenna (a) and its radiation pattern at 10 GHz (b).

The bi-static reflectarray measurement requires a setup with minimal interference from the measurement instruments. The whole measurement setup is shown in Figure 9. The components of the setup and their effect on the measurements are described below.

The array was illuminated with a linearly polarized Fermi antenna [13] with 30° 3 dB beamwidth in both E- and H-planes, see Figure 10. The latter was milled from 1.6 mm FR-4 and has low radar cross section thus minimizing the interference. The Fermi antenna was positioned at a distance of 1.35 m from the array in order to ensure uniform excitation of the screen. It is also important that the front-to-back ratio of the antenna is below 30 dB which ensures that the signal transmitted by the illuminating antenna does not interfere with the one reflected from the screen.

Both the array and illuminating Fermi antenna were placed on a rotating foam fixture, see Figure 11. We assume that permittivity of the foam is close to the one of the air. The fixture allowed changing the excitation polarization by 90° rotation of the Fermi antenna yet preserving the phase centre of the latter as shown in Figure 12. The response of the reflectarray was measured with a 20 dB dual-polarized horn placed at 6 m distance.

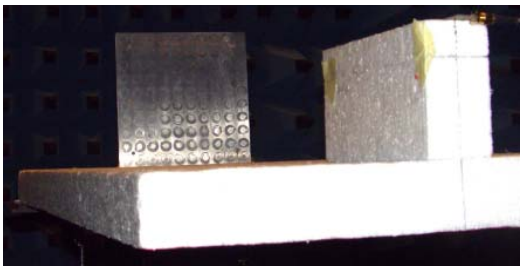

Figure 11. Rotating fixture with the reflectarray under test and the Fermi antenna.

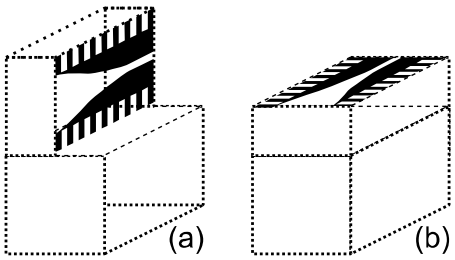

Figure 12. Fixture arrangment for measuring both vertical (a) and horizontal (b) polarization preserving position of the phase centre of the Fermi antenna.

The bi-static far-field measurement of four combinations of vertical (V) and horizontal (H) polarization excitation and response, i.e. VV, VH, HV, and HH, were performed and mathematically combined to produce the CP response, e.g. [9]. The results of the measurements are in good agreement with the simulated ones as demonstrated in Figure 13. One can

clearly observe the distinctive null in the centre of the radiation pattern, predicted in Figure 8. The null is more than 11 dB below than the two peaks around it. The discrepancies observed between the simulated and measured results are attributed to both the reflections from the anechoic chamber and the cable interference. The cable feeds the Fermi antenna and does not affect the illuminating field; however it can act as spurious scatterer when it is parallel to the polarization of the received field, see Figure 11.

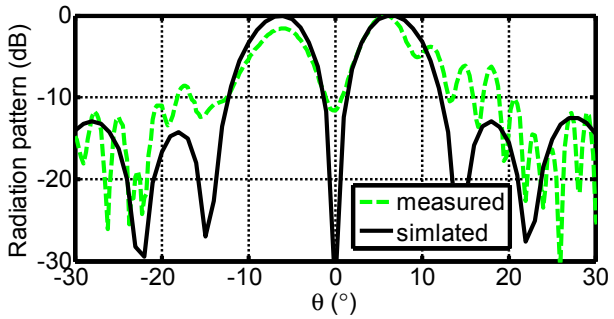

Figure 13. Comparison of simulated and measured LHCP field in xz-plane scattered from the structure excited by LHCP plane wave at 10 GHz.

V. CONCLUSIONS

The paper presents a quasi-periodic reflectarray with spiral phase distribution for the generation of helical far-field radiation patterns with circular polarization properties. The reflectarray is a flat low-profile alternative to 3D dielectric spiral phase plate or a reflector with a spiral surface profile.

Double split ring slot FSS is used as a means for adjusting the phase produced with the element rotation across the reflectarray. Simulations presented demonstrate generation of reflected helical beams at 10 GHz for circularly polarized wave incident on the structure. The far-field measurements are in a good agreement with the simulations and demonstrate a null of -11 dB in the centre of the radiation pattern attributed to the helical wavefront.

ACKNOWLEDGMENT

The authors wish to thank Mr Jim Knox for manufacturing of the reflectarray and Mr Michael Major for his help with the measurements.

REFERENCES

[1] M. Padgett and L. Allen, "Light with a twist in its tail," *Contemporary Physics*, vol. 41, no. 5, pp. 275–285, Sep. 2000.

[2] B. Jack, J. Leach, J. Romero, S. Franke-Arnold, M. Ritsch-Marte, S. Barnett, and M. Padgett, "Holographic Ghost Imaging and the Violation of a Bell Inequality," *Physical Review Letters*, vol. 103, no. 8, pp. 1–4, Aug. 2009.

[3] F. Tamburini, E. Mari, B. Thidé, C. Barbieri, and F. Romanato, "Experimental verification of photon angular momentum and vorticity with radio techniques," *Applied Physics Letters*, vol. 99, no. 20, p. 204102, 2011.

[4] G. A. Turnbull, D. A. Robertson, G. M. Smith, L. Allen, and M. J. Padgett, "The generation of free-space Laguerre-Gaussian modes at millimetre-wave frequencies by use of a spiral phaseplate," *Optics Communications*, vol. 127, no. 6, pp. 183–188, Jun. 1996.

[5] F. Tamburini, E. Mari, A. Sponselli, B. Thidé, A. Bianchini, and F. Romanato, "Encoding many channels on the same frequency through radio vorticity: first experimental test," *New Journal of Physics*, vol. 14, no. 3, p. 033001, Mar. 2012.

[6] W. Shu, D. Song, Z. Tang, H. Luo, Y. Ke, X. Lü, S. Wen, and D. Fan, "Generation of optical beams with desirable orbital angular momenta by transformation media," *Physical Review A*, vol. 85, no. 6, p. 6, Jun. 2012.

[7] R. C. Jones, "A New Calculus for the Treatment of Optical Systems. I," *Journal of the Optical Society of America*, vol. 31, no. 7, pp. 488–493, Jul. 1941.

[8] A. G. Fox, "An Adjustable Wave-Guide Phase Changer," *Proceedings of the IRE*, vol. 35, no. 12, pp. 1489–1498, Dec. 1947.

[9] R. H. Phillion and M. Okoniewski, "Lenses for Circular Polarization Using Planar Arrays of Rotated Passive Elements," *IEEE Transactions on Antennas and Propagation*, vol. 59, no. 4, pp. 1217–1227, Apr. 2011.

[10] A. E. Martynyuk, J. I. M. Lopez, and N. A. Martynyuk, "Spiraphase-Type Reflectarrays Based on Loaded Ring Slot Resonators," *IEEE Transactions on Antennas and Propagation*, vol. 52, no. 1, pp. 142–153, Jan. 2004.

[11] V. Fusco, "Mechanical beam scanning reflectarray," *IEEE Transactions on Antennas and Propagation*, vol. 53, no. 11, pp. 3842–3844, Nov. 2005.

[12] C. A. Balanis, *Antenna Theory: Analysis and Design*, 2nd ed. John Wiley & Sons, Inc., 1997, p. 960.

[13] J. B. Rizk and G. M. Rebeiz, "Millimeter-wave Fermi tapered slot antennas on micromachined silicon substrates," *IEEE Transactions on Antennas and Propagation*, vol. 50, no. 3, pp. 379–383, Mar. 2002.